

Document Version

Final published version

Citation (APA)

Sagar, S., Popovich, V., Kömmelt, P., & Dey, P. (2021). Combined Ab Initio and Experimental Study of Hydrogen Sorption in Dual-Phase Steels. In *TMS 2021 150th Annual Meeting and Exhibition Supplemental Proceedings* (pp. 730-741). (Minerals, Metals and Materials Series; Vol. 5). Springer. https://doi.org/10.1007/978-3-030-65261-6_66

Important note

To cite this publication, please use the final published version (if applicable).
Please check the document version above.

Copyright

In case the licence states "Dutch Copyright Act (Article 25fa)", this publication was made available Green Open Access via the TU Delft Institutional Repository pursuant to Dutch Copyright Act (Article 25fa, the Taverne amendment). This provision does not affect copyright ownership.
Unless copyright is transferred by contract or statute, it remains with the copyright holder.

Sharing and reuse

Other than for strictly personal use, it is not permitted to download, forward or distribute the text or part of it, without the consent of the author(s) and/or copyright holder(s), unless the work is under an open content license such as Creative Commons.

Takedown policy

Please contact us and provide details if you believe this document breaches copyrights.
We will remove access to the work immediately and investigate your claim.

Green Open Access added to TU Delft Institutional Repository

'You share, we take care!' - Taverne project

<https://www.openaccess.nl/en/you-share-we-take-care>

Otherwise as indicated in the copyright section: the publisher is the copyright holder of this work and the author uses the Dutch legislation to make this work public.

Combined Ab Initio and Experimental Study of Hydrogen Sorption in Dual-Phase Steels



Saurabh Sagar, Vera Popovich, Pascal Kömmelt, and Poulumi Dey

Abstract Controlling the detrimental effect of hydrogen on the mechanical behaviour of advanced high strength steels is decisive for their application. Precipitates in steels can be useful in irreversibly trapping the hydrogen atoms, thereby preventing their diffusion to critical regions in the microstructure where they can be most detrimental. In this work, the capability of precipitates of transition metals in limiting the amount of diffusible hydrogen has been examined. A combined ab initio–experimental approach was used to study the hydrogen sorption in two DP800 steel grades with different concentrations of titanium and vanadium using cyclic voltammetry. Under the same charging conditions, diffusible hydrogen concentration was found to be higher in the vanadium grade as compared to the titanium grade. Scanning electron microscope characterisation revealed a more compact layer of oxide on the vanadium grade which contributed to more hydrogen absorption on the surface. Density Functional Theory calculations were performed to determine the trapping strength of precipitates of titanium and vanadium. C vacancy in titanium carbide was found to be the strongest hydrogen trap, but the C vacancy formation energy was much lower in vanadium carbide. At finite temperatures, however, both precipitates are experimentally known to be off-stoichiometric. Our DFT-based finding of the titanium grade being irreversible hydrogen trap is thus in agreement with the experimental results.

S. Sagar (✉) · V. Popovich · P. Dey
Department of Materials Science and Engineering, TU Delft, Delft, The Netherlands
e-mail: s.sagar@tudelft.nl

V. Popovich
e-mail: V.Popovich@tudelft.nl

P. Dey
e-mail: P.Dey@tudelft.nl

P. Kömmelt
Tata Steel Europe, Amsterdam, The Netherlands
e-mail: pascal.kommelt@tatasteelurope.com

Keywords Advanced high strength steels · Hydrogen trapping · Cyclic voltammetry · Density functional theory

Introduction

Advanced High Strength Steels are widely used for manufacturing structural components in the automotive industry owing to their high strength and ductility [1, 2]. It has been well documented that when hydrogen is absorbed in steels, even in small concentrations of the order of 1 ppm, it causes a severe loss in strength and ductility [3–6]. The intricate phenomena of deterioration of mechanical properties of a material in the presence of hydrogen is commonly referred as hydrogen embrittlement (HE). The exact role of hydrogen in causing embrittlement is ambiguous and various mechanisms of embrittlement have been proposed to explain instances of hydrogen embrittlement [7]. However, it is understood that diffusible hydrogen which can evolve out from specimens during exposure at service temperature is responsible for HE of high strength steels [6]. Diffusible hydrogen tends to migrate towards critical regions in the microstructure such as the crack tip zone or voids surrounding inclusions, where it exerts its deleterious effect. One possible solution to improving a material's resistivity to hydrogen embrittlement is to limit the amount of diffusible hydrogen by introducing benign hydrogen *traps* in the microstructure [6, 8].

Microstructural features such as defects or impurities play a crucial role in HE. A hydrogen atom interacts with the distinct electrostatic fields around defects and can possibly bind to such a location. When the hydrogen atom is strongly bound at a site, such that it does not diffuse out upon the applied conditions of stress and temperature, it is said to be irreversibly trapped. On the other hand, reversibly trapped hydrogen atoms can diffuse out at ambient conditions and contribute to embrittlement. The distinction between a reversible and irreversible trap is not exact and depends upon the environment that the material is in. However, it has been established that defects such as grain boundaries and dislocations are reversible traps [9, 10], while second phase particles such as precipitates of alloying elements may be irreversible traps depending upon several factors such as size, stoichiometry and type of interface [11, 12]. It has been reported in a number of experimental studies [11, 13] that steels with uniform distributions of fine carbide and nitride precipitates indeed have a lower susceptibility to HE. Therefore, carbides and nitrides of transition metals seem to be prime candidates for improving resistivity to HE of steels and consequently significant research has been dedicated to this aspect. Takahashi et al. directly imaged hydrogen isotopes in VC and TiC precipitates using atom probe tomography [14]. These studies revealed that most hydrogen atoms are located within the precipitate and along the broad interfaces of these precipitates. Laureys et al. [12] compared the trapping capability of TiC and VC precipitates through hot and melt extraction in generic Fe-C-Ti and Fe-C-V steel specimen. It was observed that hydrogen was trapped more strongly in Fe-C-Ti than in the Fe-C-V alloy, indicating that TiC was a stronger trap. However, a direct comparison of trapping capacity of TiC and VC

precipitates could not be obtained through these methods. In a first-principles study on the interaction of hydrogen with TiC precipitates in α -Fe, Di Stefano et al. found that a large variety of possible trapping sites for hydrogen are possible [15]. Such sites can be associated with the particle-matrix interface, misfit dislocation cores and other defects at the interface as well as interstices and carbon vacancies within the precipitate. Trapping at the semi-coherent interfaces was moderate while carbon vacancies in the interior of the precipitate were the strongest traps.

While atomistic simulations have been able to provide fundamental insights into the trapping of hydrogen, a direct correlation between the theoretical and experimental findings has not been established thus far. In the present work, we validate the potential usability of precipitates of titanium and vanadium in irreversibly trapping absorbed hydrogen in dual-phase steels, thereby limiting the amount of diffusible hydrogen. Trapping of hydrogen in TiC, TiN, VC and VN was studied using Density Functional Theory (DFT)-based ab initio calculations and the precipitate with better trapping efficiency was identified. Simultaneously, two steel grades with different concentrations of titanium and vanadium were loaded with hydrogen under the same conditions and the amount of diffusible hydrogen was subsequently measured using Cyclic Voltammetry (CV). CV has recently been applied for measuring diffusible hydrogen in electrochemically hydrogen charged specimen [16–18]. The method is relatively fast and simple and can be performed with in situ hydrogen charging, which is a big advantage over hot extraction methods in which a large proportion of hydrogen can diffuse out between the charging and measurement steps [18].

Materials and Methods

Two commercial grades of DP800 steel with different concentrations of titanium and vanadium were chosen for this study. The chemical composition of the two grades is listed in Table 1. As can be seen, the grade with higher titanium concentration has been referred to as T-Grade while the other is called V-Grade. By selecting steel grades with these specific compositions, it was possible to ensure that a high number density of titanium carbides and nitrides would be present in the T-grade and similarly vanadium precipitates in V-grade. Carbides in dual phase steel are known to be in the size range of 4 nm up to 50 nm for (semi) coherent nano-precipitates while incoherent precipitates ranging up to 150 nm have been reported [19, 20].

Dual-phase (DP) steels studied herein have a microstructure of mainly soft ferrite with islands of hard martensite dispersed throughout the matrix. For both materials,

Table 1 Concentration of elements of interest in the two DP800 steel grades

	C (wt%)	N (ppm)	Ti (wt%)	V (wt%)
Grade T	0.148	45	0.020	0.004
Grade V	0.158	44	0.009	0.062

grain sizes were in the range of 5–10 μm . Semi-quantitative XRD analysis of the steel samples revealed a microstructure consisting of $4 \pm 1\%$ retained austenite for both grades.

Experimental Approach

CV experiments with in situ hydrogen charging were conducted on both materials to compare the amount of diffusible hydrogen sorbed under specified charging conditions. The as-received material had been hot-dip galvanised beforehand. For performing electrochemical experiments, the steel specimens were de-coated by immersing in 1:1 HCl solution following which they were rinsed with isopropanol. One side of the sample, which was to be exposed to the electrolyte was sanded and polished to a surface finish of 1 μm . A three-electrode setup was used with the steel sample as the working electrode, a double junction saturated Ag/AgCl reference electrode (+0.197 V versus SHE) and a platinum mesh as counter electrode. A circular area of diameter 1 cm on the sample surface was exposed to the electrolyte. The electrolyte consisted of a solution of 8 g/l thiourea in 1 M NaOH. Thiourea is an organo-sulphur compound with the formula $\text{SC}[\text{NH}_2]_2$ which is known to function as a recombination poison. It facilitates the retention of protons in the electrolyte during the test thereby promoting the ability of atomic hydrogen to enter steel.

Electrochemical measurements were performed with a Bio-Logic VSP300 potentiostat. The test consisted of three steps—(i) two initial cyclic voltammetry scans from -1.25 V to -0.2 V at a scan rate of 10 mV/s. The first scan was done to ensure that the sample surface was consistent for all tests, while the second scan was used to generate a baseline. (ii) Immediately after the second CV scan, cathodic hydrogen charging was carried out by applying a constant potential of -1.25 V. Charging was done for three different durations of 30, 60 and 120 min. (iii) For detecting the absorbed hydrogen, hydrogen charging was followed by two CV scans. For quantifying the amount of hydrogen, instead of the CV scans, a static potential of -0.9 V versus Ag/AgCl was applied to the cell after hydrogen charging. The choice of this potential was based on results from CV experiments and will be explained later. Three sets of tests were performed for each grade.

Theoretical Approach

DFT calculations were performed to compute the trapping efficiency of TiC, TiN, VC and VN. All DFT calculations were carried out using the Vienna Ab initio simulation package (VASP) [21, 22]. The generalised gradient approximation (GGA) parameterised by Perdew, Burke and Ernzerhof [23] was employed for exchange correlation. The Methfessel-Paxton method [24] with a smearing width of 0.15 eV has been used for the Fermi surface smearing. The single-electron wave functions

were expanded by using plane waves up to an energy cutoff of 500 eV. All lattice vectors and atomic positions were relaxed until the residual forces acting on each atom were below 0.01 eV/Å. An energy tolerance of 10^{-6} eV was defined as a convergence criterion for the self-consistent electronic loop. The Brillouin zone was sampled using Monkhorst-Pack grids [25] with a $24 \times 24 \times 24$ grid for the 8 atom unitcell and $6 \times 6 \times 6$ grid for the 64 atom supercell.

The formation energy of studied compounds was calculated as the difference between the total energy of the compound phase and that of its constituent elements. Equation 1 depicts this relation, where M is the metal atom, X is a carbon or nitrogen atom and a and b are the number of atoms of the two constituents of the compound.

$$E_f = E[M_a X_b] - aE[M] - bE[X] \quad (1)$$

To determine the propensity of the compounds to form vacancies, the vacancy formation energy was calculated as:

$$E_v = E[MX_{\text{vacancy}}] - E[MX_{\text{perfect}}] + \mu_X^0 \quad (2)$$

where μ_X^0 is the chemical potential of an X atom in BCC iron. Hydrogen trapping was characterised by the solution energy of hydrogen at a trap site. Solution energy was calculated at interstitial sites and vacancies according to:

$$E_H = E[MXH] - E[MX] - \frac{1}{2}\mu_{H_2}^0 \quad (3)$$

where $\mu_{H_2}^0$ is the ground state energy of a hydrogen molecule. The energies used in Eqs. 1, 2 and 3 were obtained from DFT calculations.

Results and Discussion

Experimental Results

The voltammograms obtained for the both materials, before and after hydrogen charging are shown in Fig. 1. The shape of the voltammogram was similar for both materials which was to be expected owing to the similarity in composition of the materials. For the uncharged specimen, two peaks were formed in the anodic direction. The first peak, labelled as A1 occurs at a potential of -0.86 V. This peak was also observed in the work of Ozdirik et al. and was determined to be arising from thiourea related oxidation processes [18]. The second peak, A2, was observed at a potential of -0.7 V and is attributed to the oxidation of iron. Oxidation of iron was visible on the sample as a reddish-brown layer over the exposed area. When the sweep direction was reversed, peak B1 formed in the cathodic branch at a potential

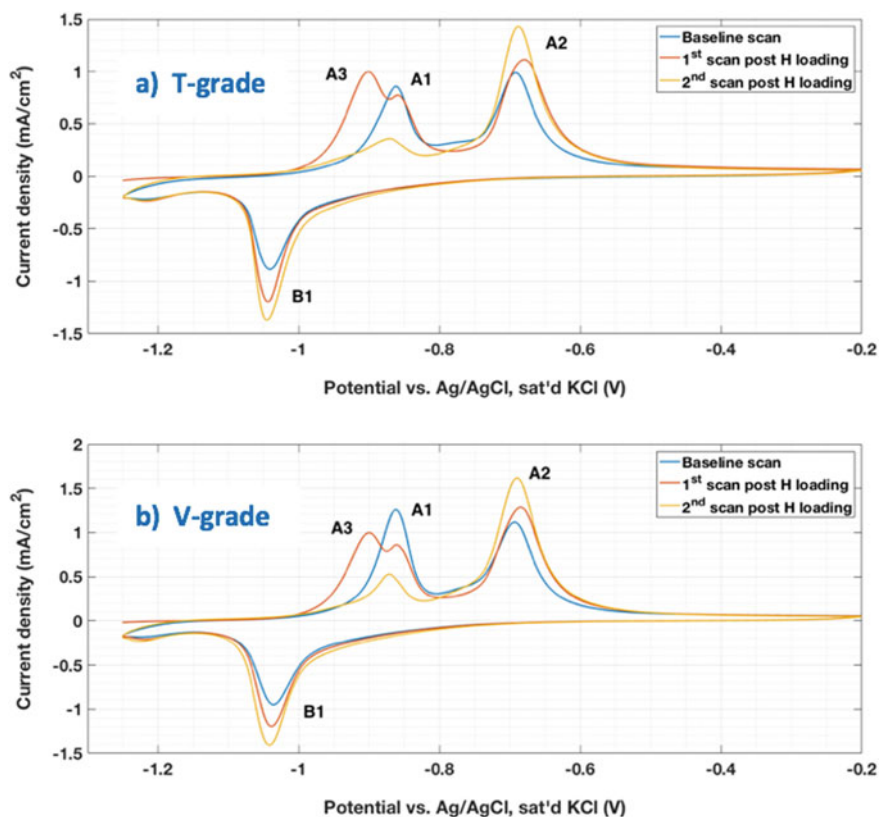


Fig. 1 CV plots obtained a T-grade and a V-grade sample. Baseline scan was done on uncharged samples followed by two scans after 30 min of hydrogen charging. (Color figure online)

of -1.04 V. The areas of peak A2 and B1 were found to be quite similar. Thus, peak B1 was arising due to the reduction of iron which was oxidised during the forward scan.

For the hydrogen charged samples, peaks A1, A2 and B1 occurred at exactly at the same potentials as the uncharged case. However, a previously unknown peak A3 was formed at a potential of -0.9 V for both materials. This potential corresponds to the evolution of hydrogen. During the charging step, hydrogen was evolved from the electrolyte. The hydrogen atoms were first adsorbed or chemisorbed on the sample surface and subsurface followed by diffusion into the bulk where it may get trapped. Thus, peak A3 is attributed to diffusible hydrogen that is desorbed from the specimen. Hydrogen that is detected via this method includes contributions from surface and subsurface sites and possibly reversible traps, such as grain boundaries, in the bulk of the specimen. Upon subsequent scanning, the hydrogen related peak disappeared, which suggested that hydrogen was completely desorbed during the previous scan. Peak A1 which was attributed to thiourea is also diminished significantly. This is to

be expected as some thiourea from the electrolyte is consumed to prevent hydrogen recombination.

For quantification of the absorbed hydrogen, current transients obtained from the potentiostatic discharging step were integrated. The potential was chosen as -0.9 V, which was the potential at which the hydrogen peak had formed. Although discharging was done for a duration of 30 min, after an instantaneous rise in current, it began to drop significantly and within 100 s, it was almost zero. For this reason, the current-time plot was integrated up to 100 s. The surface charge density thus obtained was divided by the charge on an electron to obtain the number density of electrons. As each electron reacts with one hydrogen atom, the number of hydrogen atoms is equal to that of electrons. The number density of hydrogen atoms was then divided by the atomic density of iron to yield the concentration of hydrogen in atomic ppm. A comparison of hydrogen content with charging duration for the two materials is presented in Fig. 2. The observed diffusible hydrogen content in V-grade steel was consistently higher (by around 25%) than in T-grade. Since the phase compositions are similar for both materials, the bulk diffusion constants for hydrogen in both materials is expected to be the same. Hence, kinetics of diffusion does not play a role in the observed difference in hydrogen concentration. It is also notable that the scatter in values obtained for T-grade was consistently higher than that in V-grade.

SEM imaging of the sample post experiments revealed an oxide layer on both materials are shown in Fig. 3. The thickness of the oxide layer was around $2\ \mu\text{m}$ for both materials. However, V-grade steels exhibited a uniform oxide layer throughout the activated area while that for T-grade steels was sparse and irregular. Upon contrasting the oxide film morphology against the measured hydrogen content, it was seen that the material with a larger scatter in data had a more irregular oxide morphology. As the oxide layer on T-grade was more susceptible to irregularities, the number density of hydrogen trap sites on the surface would also vary significantly between multiple samples, which possibly led to a large scatter in the

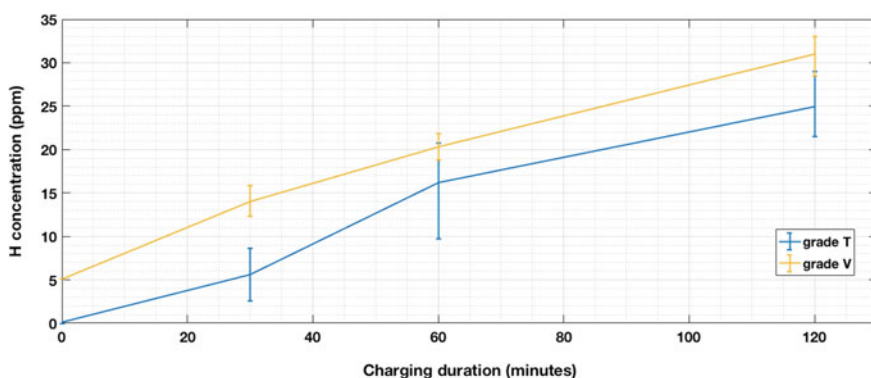


Fig. 2 Comparison of diffusible hydrogen content in both grades as measured from potentiostatic discharging experiments. Hydrogen content in V grade was consistently higher than in T grade samples. (Color figure online)

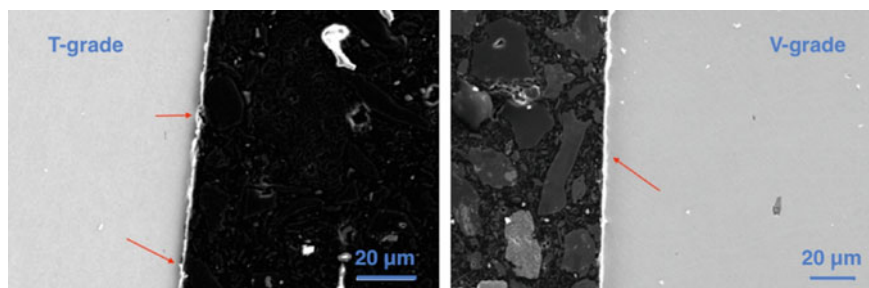


Fig. 3 Oxide layer morphology on samples of both grades. The arrows on T-grade indicate voids at the oxide-metal interface. (Color figure online)

measured hydrogen content. This observation therefore offers evidence for trapping of hydrogen by the oxide layer. Additionally, the dense layer on V-grade would offer more trap sites, and correspondingly, more hydrogen was absorbed by this grade.

DFT Results

Both titanium carbide/nitride and vanadium carbide/nitride crystallise in the rock salt crystal structure (Fig. 4). The equilibrium lattice parameters, formation energy and vacancy formation energy obtained for the four compounds are listed in Table 2. The values obtained for lattice parameter and formation enthalpy are comparable with previously reported works [26–28] and the references used therein. The formation of each compound is exothermic indicating the phases are stable. However, the vacancy formation energy in both titanium compounds as well as VN is endothermic, indicating that these compounds would remain stoichiometric (with respect to C and N) in the absence of any kind of applied plastic strain and at zero temperature. This

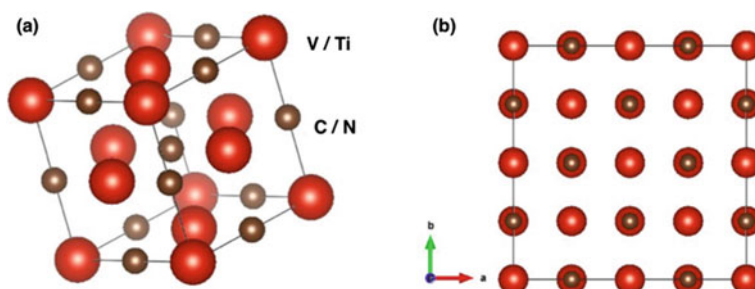


Fig. 4 **a** Unit cell of the studied compounds depicting the rocksalt type crystal structure. Simulations were carried out on $2 \times 2 \times 2$ supercells **(b)** generated by repeating the unit cells twice along each lattice vector. (Color figure online)

Table 2 Structural parameters and energies of the studied compounds from calculations on a $2 \times 2 \times 2$ supercell

Parameter	Compound			
	TiC	VC	TiN	VN
Lattice Constant (Å)	4.33	4.15	4.25	4.12
Structure Formation Energy (eV/f.u)	-9.44	-6.32	-14.08	-8.16
Vacancy Formation Energy (eV)	1.29	-0.24	2.44	1.16

is in contrast to VC, which is known to precipitate in the off-stoichiometric V_4C_3 composition [29].

Hydrogen solution energies in the studied compounds were firstly calculated at the interstitial sites. As the octahedral sites are fully occupied by C or N atoms, only the tetrahedral sites can accommodate hydrogen atoms. As can be seen from Table 3, hydrogen solubility at interstitial sites was endothermic, indicating that occupation of these sites by hydrogen is a thermally activated process. Hydrogen solubility in a C/N vacancy within the precipitate was also calculated according to Eq. 3. Hydrogen solution energy is negative for all compounds, indicating exothermic dissolution in vacancies. Comparison with interstitial sites clearly shows that vacancies within a precipitate are stronger traps for a hydrogen atom as compared to tetrahedral interstices. A carbon vacancy in TiC is seen to have the strongest affinity for hydrogen. Vacancy-hydrogen complex formation energy is the energy required to form a C/N vacancy in the compound and the energy required to dissolve a hydrogen atom in the vacancy. The C vacancy formation in VC was found to be exothermic, unlike the other compounds (refer to Table 2).

The values obtained for vacancy-hydrogen complex formation energy would suggest that irreversible trapping during hydrogen charging should be more effective in the V-grade material, and consequently, the amount of diffusible hydrogen should be lesser than the T-grade. This is, however, in contradiction to the experimental results. Following are the key factors for the observed contradiction between theory and experiments. It has already been mentioned that the oxide layer is contributing to some reversible hydrogen trapping which can alter the results of the experiments. Other possible reasons are the finite temperature effects and/or the elastic strain between coherent precipitates and matrix. To elaborate, C (N) vacancy formation is energetically feasible at finite temperatures because of configurational entropy, which

Table 3 Hydrogen trapping related energetics in studied compounds for a $2 \times 2 \times 2$ supercell

Parameter	Compound			
	TiC	VC	TiN	VN
H-Solution energy in interstices (eV)	1.33	1.99	2.30	1.23
H-Solution energy in vacancy (eV)	-0.96	-0.06	-0.38	-0.26
Vacancy-H complex formation energy (eV)	0.33	-0.30	2.06	0.90

holds true for both Ti and V precipitates. Furthermore, the elastic strain between coherent precipitates embedded in matrix plays a significant role in driving out C or N atoms from the precipitates to the surrounding matrix, even at zero temperature. Hence, Ti and V precipitates are expected to be off-stoichiometric with respect to C or N. It is worthwhile to mention here that the Ti or V precipitates are indeed experimentally observed to be off-stoichiometric [29, 30]. This implies that the DFT-based finding of TiC and TiN precipitates being stronger hydrogen traps than their V counterpart is consistent with the experimental observation.

Conclusions

This work was focused on examining the capability of precipitates in trapping hydrogen thereby limiting the amount of diffusible hydrogen in the material. CV results showed that the amount of diffusible hydrogen after two hours of hydrogen charging was approximately 25% higher in V-grade steel than in T-grade steel. However, the method has a shortcoming since the oxide layer formed during CV scans can also contribute to reversible trapping of hydrogen. It is thus recommended that for establishing the method for measuring hydrogen sorption, the contribution of oxide layer to trapping needs to be quantified. DFT calculations were carried out to compare the hydrogen trapping efficiency of carbides and nitrides of vanadium and titanium. It was observed that H solubility in interstitial sites was endothermic, indicating that trapping was unfavourable. However, H solubility in a C/N vacancy was found to be exothermic. C vacancy in TiC was found to be the stronger trap than that in VC (-0.91 eV versus -0.06 eV for VC). This was, however, counterbalanced by the high C vacancy formation energy in TiC. It is noteworthy that both compounds are experimentally known to be off stoichiometric. It is thus concluded from our combined ab initio—experimental approach that the contribution of precipitates of Ti in irreversible hydrogen trapping is higher in T-grade steel, than the corresponding role played by V precipitates in the V-grade steel.

Acknowledgements We would like to thank Tata Steel Europe for supporting the work through knowledge sharing and providing materials for the study.

References

1. Horvath CD (2010) Advanced steels for lightweight automotive structures. In *Materials, design and manufacturing for lightweight vehicles*. Woodhead Publishing Series in Composites Science and Engineering, pp 35–78
2. Hilditch T, de Souza T, Hodgson P (2015) Properties and automotive applications of advanced high-strength steels (AHSS). In *Welding and joining of advanced high strength steels (AHSS)*. Woodhead Publishing, Cambridge, pp 9–28

3. Fan D, Pielet H (2018) Bend failure mechanism of zinc coated advanced high strength steel. *ISIJ Int* 58:1528–1544
4. Hagihara Y, Shobu T, Hisamori N, Suzuki H, Takai K, Hirai K (2012) Delayed fracture using CSRT and hydrogen trapping characteristics of V-bearing high-strength steel. *ISIJ Int* 52(2):298–306
5. Mohtadi-Bonab M, Eskandari M, Rahman K, Ouellet R, Szpunar J (2016) An extensive study of hydrogen-induced cracking susceptibility in an API X60 sour service pipeline steel. *Int J Hydrogen Energy* 41:4185–4197
6. Takai K, Watanuki R (2003) Hydrogen in trapping states innocuous to environmental degradation of high-strength steels. *ISIJ Int* 43(4):520–526
7. Barrera O, Bombac D, Chen Y, Daff T, Galindo-Nava E, Gong P, Haley D, Horton R, Katzarov I, Kermodie J, Liverani C, Stopher M, Sweeney F (2018) Understanding and mitigating hydrogen embrittlement of steels: a review of experimental, modelling and design progress from atomistic to continuum. *J Mater Sci* 53:6251–6290
8. Bhadeshia H (2016) Prevention of hydrogen embrittlement in steels. *ISIJ Int* 56(1):24–36
9. McEniry EJ, Hickel T, Neugebauer J (2017) Hydrogen behaviour at twist {110} grain boundaries in α -Fe. *Philosophical Trans Royal Soc A* 375(2098)
10. Hagi H, Hayashi Y (1987) Effect of dislocation trapping on hydrogen and deuterium diffusion in iron. *Trans Jpn Inst Met* 28(5):368–374
11. Cui Q, Wu J, Xie D, Wu X, Huang Y, Li X (2017) Effect of nanosized NbC precipitates on hydrogen diffusion in X80 pipeline steel. *Materials* 10(7)
12. Laureys A, Claeys L, Seranno TD, Depover T, Eeckhout EVd, Petrov R, Verbeken K (2018) The role of titanium and vanadium based precipitates on hydrogen induced degradation of ferritic materials. *Mater Charact* 144:22–34
13. Valentini R, Solina A, Matera S, De Gregorio P (1996) Influence of titanium and carbon contents on the hydrogen trapping of microalloyed steels. *Metall Mater Trans A* 27:3773–3780
14. Takahashi J, Kawakami K, Kobayashi Y, Tarui T (2010) The first direct observation of hydrogen trapping sites in TiC precipitation-hardening steel through atom probe tomography. *Scripta Mater* 63(3):261–264
15. Stefano DD, Nazarov R, Hickel T, Neugebauer J, Mrovec M, Elsässer C (2016) First-principles investigation of hydrogen interaction with TiC precipitates in alpha-Fe. *Phys Rev B* 93(18)
16. Uluc V (2015) Hydrogen sorption and desorption properties of Pd-alloys and steels investigated by electrochemical methods and mass spectrometry. TU Delft, Netherlands
17. Flores KSE (2019) Study of hydrogen sorption/desorption effect on austenitic iron-based alloys. TU Delft, Netherlands
18. Ozdirik B, Depover T, Vecchi L, Verbeken K, Terryn H, Graeve ID (2018) Comparison of electrochemical and thermal evaluation of hydrogen uptake in steel alloys having different microstructures. *J Electrochem Soc* 165(11):787–793
19. Kamikawa N, Hirohashi M, Sato Y, Chandiran E, Miyamoto G, Furuhashi T (2015) Tensile behavior of ferrite-martensite dual phase steels with nano-precipitation of vanadium carbides. *ISIJ Int* 55(8):1781–1790
20. Li CH, Chen CY, Tsai SP, Yang (2019) Microstructure characterization and strengthening behavior of dual precipitation particles in Cu-Ti microalloyed dual-phase steels. *Mater Design* 166
21. Kresse G, Hafner J (1993) Ab initio molecular dynamics for open-shell transition metals. *Phys Rev B* 48(17):13115–13118
22. Kresse G, Furthmüller J (1996) Efficient iterative schemes for ab initio total-energy calculations using a plane-wave basis set. *Phys Rev B* 54(16):11169–11186
23. Perdew JP, Burke K, Ernzerhof M (1996) Generalized gradient approximation made simple. *Phys Rev Lett* 77(18):3865–3868
24. Methfessel M, Paxton A (1989) High-precision sampling for Brillouin-zone integration in metals. *Phys Rev B* 40(6):3616–3621
25. Monkhorst HJ, Pack JD (1976) Special points for Brillouin-zone integrations. *Phys Rev B* 13(12):5188–5192

26. Restrepo SE, Di Stefano D, Mrovec M, Paxton AT (2020) Density functional theory calculations of iron—vanadium carbide interfaces and the effect of hydrogen. *Int J Hydrogen Energy* 45(3):2382–2389
27. Yang R, Zhu C, Wei Q, Du Z (2016) Investigations on structural, elastic, thermodynamic and electronic properties of TiN, Ti₂N and Ti₃N₂ under high pressure by first-principles. *J Phys Chem Solids* 98:10–19
28. Li H, Zhang L, Zeng Q, Guan K, Li K, Ren H, Liu S, Cheng L (2011) Structural, elastic and electronic properties of transition metal carbides TMC (TM = Ti, Zr, Hf and Ta) from first-principles calculations. *Solid State Commun* 151(8):602–606
29. Epicier T, Acevedo D, Perez M (2008) Crystallographic structure of vanadium carbide precipitates in a model Fe-C-V steel. *Phil Mag* 88(1):31–45
30. Dong B-X, Qiu F, Li Q, Shu S-L, Yang H-Y, Jiang Q-C (2019) The synthesis, structure, morphology characterizations and evolution mechanisms of nanosized titanium carbides and their further applications. *Nanomaterials* 9(1152)